

SYNTHESIS OF Co DOPING SrMoO₄ FOR ENHANCED PHOTOCATALYTIC PERFORMANCE VIA HYDROTHERMAL METHOD

L. Y. ZHANG^{a,b,*}, G. H. ZHENG^b, Z. X. DAI^b, X. D. ZHAO^a

^a*Department of Chemical and Material Engineering, Hefei University, Hefei 230601, China*

^b*Anhui Key Laboratory of Information Materials and Devices, School of Physics and Materials Science, Anhui University, Hefei 230039, China*

Visible-light-driven photocatalyst Co-doped SrMoO₄ was successfully synthesized by a facile hydrothermal preparation. The results showed that Co doping has not effect on the crystal structure of SrMoO₄ but plays an important role on the morphology. The photocatalytic measurements indicated that Co doping can effectively enhance the photocatalytic activities of the SrMoO₄ which were evaluated by the degradation of methyl blue (MB) under visible light irradiation. And the 5% Co-doped SrMoO₄ shows the optimal photocatalytic performance. The enhancement of photocatalytic activity is attributed to narrower band gap and the lower recombination ratio of photo-induced electron-hole pairs with Co doping.

(Received May 3, 2019; Accepted July 15, 2019)

Keywords: SrMoO₄; Co doping; photocatalyst; hydrothermal method

1. Introduction

Scheelite-structured compounds molybdates in the AMoO₄ (A=Ba, Sr or Ca) family have been attracting considerable attention in recent years owing to their attractive properties, as well as their versatile potential applications [1-6]. SrMoO₄ crystallize in this so-called scheelite structure, which belong to the tetragonal space group I41/a. The structure consists of two fundamental SrMoO₄ units, Sr and Mo have S4 point symmetry site. Each Mo is surrounded by four oxygens and forms a tetrahedron, and these tetrahedra are linked by the Sr-O bonds. On the other hand, each Sr is surrounded by eight oxygens and forms octahedral.

SrMoO₄ is regarded as one semiconductor material with wide band gap (4.0eV) and can only absorb UV light ($\lambda < 387\text{nm}$) [7]. To maximum the use of sunlight and enhance the photocatalytic activity of SrMoO₄, many methods have been developed. For example, we adopted thermal decomposition of metal-organic salt in the organic solvent to obtain the lowest energy band 2.71eV till now. The UV-absorbance spectrum suggest that larger absorption of the SrMoO₄ samples is located in the visible light region including UV light region. As a result, nearly 100% degradation efficiency for methyl blue in 120 minutes is obtained by the photocatalytic measurement [8]. Stirring speed in the hydrothermal preparation also can enhance the SrMoO₄ photocatalytic activity [9].

* Corresponding author: 522671714@qq.com

As we know, for a photocatalyst with wide band gap, the doping with a foreign element is a good way to enhance the photocatalytic activity. For example, the M doping (M=Ag, Co and Ni) into BiVO_4 can suppress the photogenerated electrons and holes and enhance the photocatalytic decomposition of organic compounds [10]. With Cr^{3+} ions doping into TiO_2 and SrTiO_3 , the photocurrent of semiconductor increase, and the photocatalytic decomposition of organic compounds is enhanced [11]. Based on the above ideas, in the present work, Co/SrMoO₄ catalysts were synthesized by a facile hydrothermal process. The band structure of SrMoO₄ was previously suggested to be composed of Mo_{4d} and hybridization of O_{2p} and Sr_{6s}. When Co²⁺ is doped into SrMoO₄ lattice, because the size mismatch between Co²⁺ is smaller for Mo⁶⁺ than for Sr²⁺, it is more likely that Co²⁺ enters Mo⁶⁺ sites. And the photocatalytic experiments suggested that the introduction of Co into SrMoO₄ is helpful for the photodegradation enhancement of methyl blue (MB). With Co doping, intermediary energy level is introduced and the band gap becomes smaller, as a result, the recombination rate of photo-induced electrons decreases and the lifetime of carriers is prolonged. Correspondingly, the photocatalytic activity is improved.

2. Experimental

Stoichiometric amounts of $\text{Sr}(\text{NO}_3)_2$, $\text{Co}(\text{NO}_3)_3$, $(\text{NH}_4)_6\text{Mo}_7\text{O}_{24}$ and NaOH were separately dissolved in the deionized water with stirring for 20 min using a magnetic stirrer. Then, the $\text{Sr}(\text{NO}_3)_2$ and $(\text{NH}_4)_6\text{Mo}_7\text{O}_{24}$ were mixed with continuous stirring. The NaOH solution was added to adjust pH values. Finally, the mixture was placed in a 1000 ml hastelloy autoclave (Parr 4577) and reacted at 120 °C for 6 h. After the autoclave was cooled to room temperature naturally, the products were separated by centrifugation, washed with ethanol and deionized water several times, and subsequently dried at 80 °C to obtain the final samples. The obtained samples, with different Co doping content (0, 0.01, 0.03, 0.05, 0.07, 0.09 and 0.11, as referred as Co--00, Co--001, Co--003, Co--005, Co--007, Co--009 and Co--011, respectively.

The crystal structures of the products were characterized by X-ray diffraction (XRD) using an X-ray diffractometer (dx-2000 SSC) with Cu $K\alpha$ radiation ($\lambda=1.5418 \text{ \AA}$) over a scanning range of 10-80° with a step of 0.02°. Using an X-ray photoelectron spectrometer (XPS, Elcalab 250 Xi, American), the valence states of ions were also tested. Scanning electron microscopy (SEM, S-4800, Hitachi) was used to observe the morphology and microstructure. UV-vis absorbance spectra detection was also performed by using a Japan Shimadzu UV-3600 (Japan) using BaSO₄ as a reference. The excitation and emission spectra were measured on a FL fluorescence spectrophotometer (F-4500, Hitachi).

The photocatalytic activity of Co/SrMoO₄ samples was evaluated by the degradation of methyl blue (MB) under a 350 W Xe lamp light. In each experiment, 200 mg of the photocatalyst was added to 80 ml of MB solution (10 mg/L) in one test tube. Before illumination, the suspensions were magnetically stirred in the dark for 1 h to ensure the establishment of an adsorption-desorption equilibrium between the photocatalyst and MB solution. And then, the solution under magnetic stirring was exposed to Xe lamp light irradiation. At given interval time, the test tubes were sampled and then centrifuged to remove the photocatalyst particles.

3. Results and discussions

3.1. XRD analysis

Due to the Co doping does not change the XRD patterns of SrMoO_4 , for simplicity, the results are not provided for all samples. Herein, we provide the XRD patterns for pure SrMoO_4 (Co--00), 5%Co-doped SrMoO_4 (Co--005) and 11%Co-doped SrMoO_4 (Co--011) samples, as shown in Fig. 1. The sharp and well-defined peaks suggest that these samples have well crystallization and no other impurities were detected. The observed pattern indicates that all of the prepared SrMoO_4 samples have pure scheelite tetragonal structure (I41/a space group), corresponding to the JCPDS 850586 [8]. The diffraction peaks of as-prepared samples correspond to the (101), (112), (004), (200), (211), (204), (220), (116), (303), (224), (400), (316), and (404) planes, as shown in Fig. 1. The XRD result implies that Co was doped into the SrMoO_4 lattice and this Co doping does not change the lattice structure of SrMoO_4 during the crystallization process.

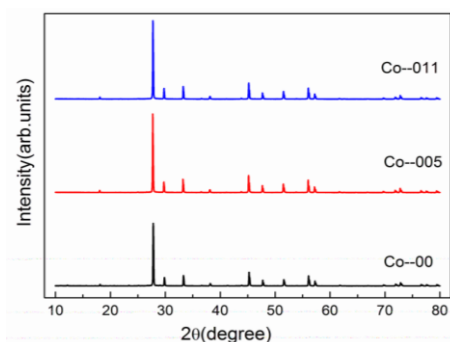


Fig. 1. XRD pattern for pure SrMoO_4 (Co--00), 5%Co-doped SrMoO_4 (Co--005) and 11%Co-doped SrMoO_4 (Co--011) samples.

Fig. 2 presents the crystal structure of SrMoO_4 . In this structure, each central Mo atom is surrounded by four equivalent O atoms, constituting one MoO_4^{2-} tetrahedral symmetry configuration. And each divalent metal atom shares corners with eight adjacent O atoms in MoO_4^{2-} tetrahedron [12]. The lattice parameters for the above five samples are calculated according to $\frac{1}{d^2} = \frac{h^2 + k^2}{a^2} + \frac{l^2}{c^2}$, where $2d \sin \theta = n\lambda$, a and c are the lattice parameters, θ is the diffraction angle, λ is the wavelength of the Cu $K\alpha$ irradiation, and (h k l) are the crystal plane indexes. The calculated lattice parameters are presented in Table 1. It is found that the lattice parameters of these samples vary with Co doping. The standard values of these lattice constants are 5.39 Å and 12.02 Å for SrMoO_4 . These variations of the lattice parameters indicate that the distortions may be introduced in the SrMoO_4 lattice. However, it can be seen that the lattice parameter changes slightly with Cr doping content, which may be ascribed to the similar lattice parameter between Co ($r=0.69\text{Å}$) and Mo ($r=0.59\text{Å}$), as discussed below.

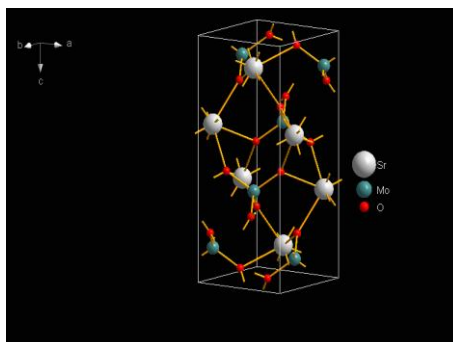


Fig. 2. Crystal structure of SrMoO_4

Table 1. The lattice parameter values for all samples.

| Sample | Co--00 | Co--001 | Co--003 | Co--005 | Co--007 | Co--009 | Co--011 |
|--------|---------|---------|---------|---------|---------|---------|---------|
| a (Å) | 5.3834 | 5.3866 | 5.3782 | 5.3794 | 5.3785 | 5.3774 | 5.3800 |
| c (Å) | 11.9553 | 12.0124 | 12.0288 | 12.0322 | 12.0364 | 12.0415 | 12.0425 |

3.2. XPS study

XPS spectra for pure SrMoO_4 (Co--00) and 5%Co-doping SrMoO_4 (Co--005) samples were measured and the results are presented. Fig. 3(a) provide the survey XPS spectra, and the obvious peaks corresponding to Sr 3d, Mo 4p, Mo 3d, Mo 3p, and O1s can be observed in both samples. The observed binding peaks of C 1s is at 283.28 eV which originates from carbon in the instrument. In addition, a weak peak of Co appears at about 788.42 eV in the 5%Co-doping SrMoO_4 . Figure 3(b)-(d) provide the high-resolution XPS spectrum of Mo, O and Co element. In Figure 3(b), these peaks centered at 235.15(235.21) eV and 232.02(232.13) eV can be assigned to Mo $3d_{3/2}$ and Mo $3d_{5/2}$ [13]. In Fig. 3(c), the peaks at binding energies of 530.06 eV for pure SrMoO_4 , and 530.15 eV for the 5%Co-doped SrMoO_4 correspond to the O 1s. To further indentify the chemical state of Co, the Co 2p high resolution XPS spectrum of 5%Co-doped SrMoO_4 is shown in Fig. 3(d). And the binding energies of 797.00 eV and 780.93 eV correspond to the Co 2p_{1/2} and Co 2p_{3/2}, respectively. It suggests that the Co element existed in form of Co^{3+} in our sample [14]. As discussed before, due to the radius of Co^{3+} (0.69 Å) was much smaller than Sr^{2+} (1.18Å), but almost similar than the radius of the Mo^{6+} (0.59 Å), it is reasonable to conclude that the doping Co^{3+} maybe replace some Mo^{6+} in the internal lattice structure of SrMoO_4 .

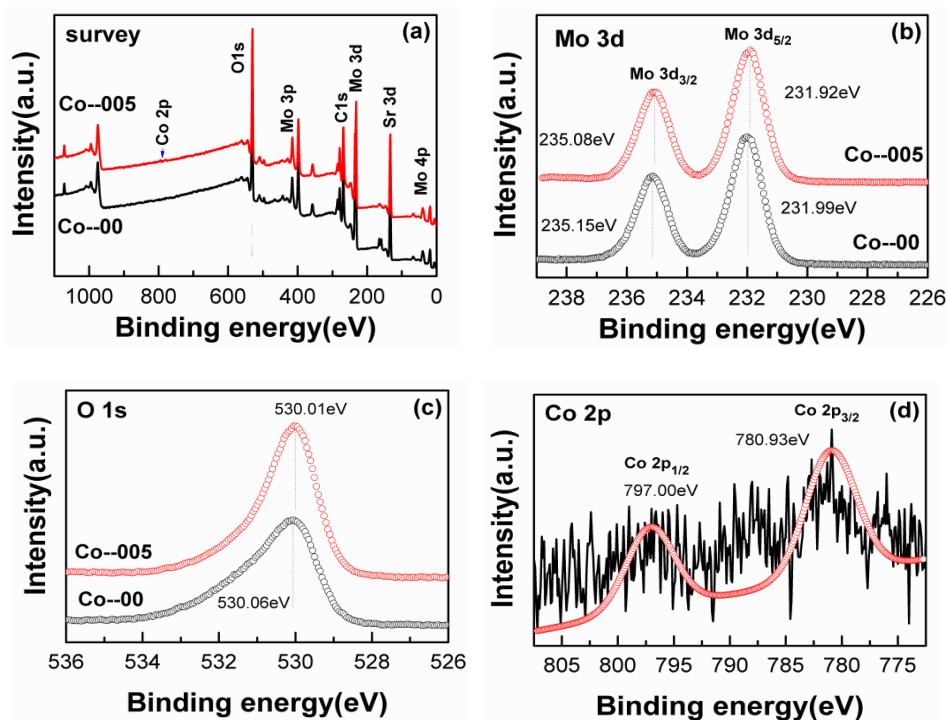


Fig. 3. Survey (a), Mo 3d (b), O 1s (c) XPS spectra for Co--00 and Co--005 samples, (d) Co 2p XPS spectra for Co--005 sample.

3.3. SEM analysis

Fig. 4 presents the SEM profiles for all samples (Co--001--a, Co--003--b, Co--005--c, Co--007--d). Till now, a number of preparation methods have been adopted to synthesis SrMoO_4 compound, such as co-precipitation reaction [15], microwave radiation [16], electrochemical process [17], hydrothermal [18], and sol-gel methods [19]. And various morphological SrMoO_4 , such as flower-like sphere, spindle rod, peanut, dumbbell, hierarchical nanosheets, nanowires, nanoplates have been obtained [20,21]. Our SEM microphology result indicate that our samples are composed of a large quantity of anisotropic microcrystals with octahedron-like and decagonal-like morphology. In addition, these octahedron and decagonal structure tend to be faceted and aligned by “docking” processes, creating an extended morphology as shown in Fig.4. In addition, for No-doping sample SrMoO_4 , the spindle-like crystals are observed (not shown here) in previous report. Obviously, the Co introduction into SrMoO_4 have effected morphology heavily [22].

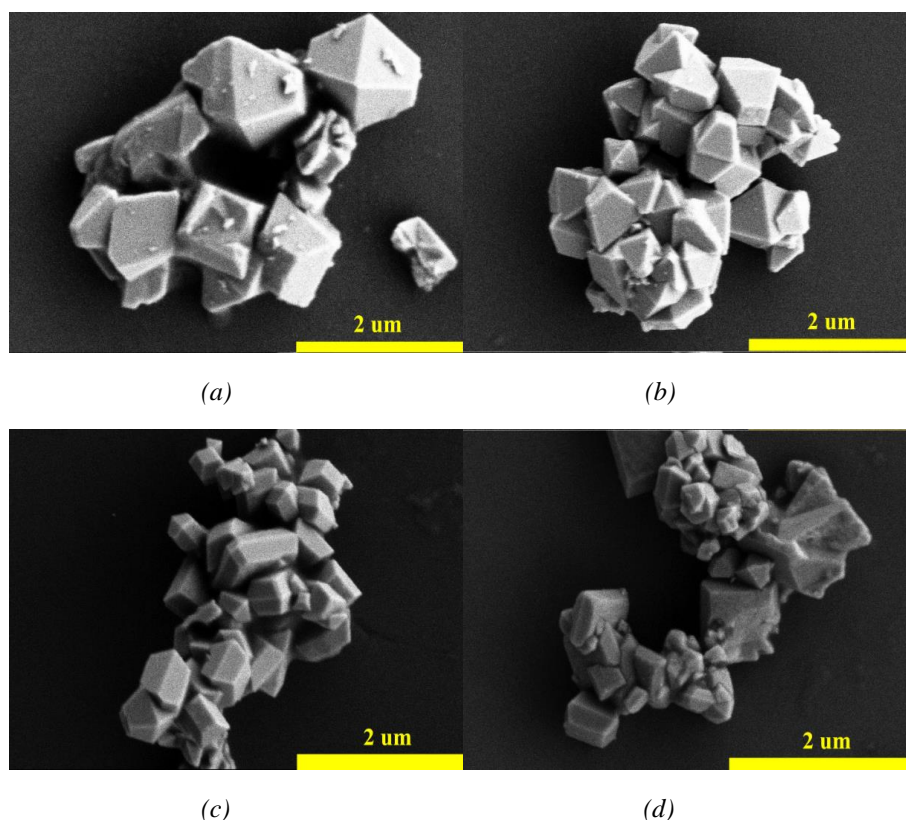


Fig. 4. SEM for Co--001 (a), Co--003(b), Co--005(c), Co--007(d) samples.

3.4. Optical properties

Fig. 5 provides the UV-visible absorption spectra of the Co--00, Co--001, Co--003, Co--005, Co--007, Co--009, Co--011 products. There exists one strong and broad absorption in the UV region (200-400nm), which is attributed to the charge transfer from the oxygen ($2p$) electrons that move into the central molybdenum atom inside the $[\text{MoO}_4]^{2-}$ ion. In addition, a hump ranging from 500 to 650nm can be observed with Co doping as shown in Fig. 5, and the reason is unclear. The optical band gap energy (E_g) is also calculated by the method proposed by Wood and Tauc [23]. The optical band gap is associated with the absorbance and the photo energy by the following equation: $\alpha h\nu = A(h\nu - E_g)^n$, where α , h , ν , E_g and A are absorption coefficient, Planck constant, photon frequency, photonic energy gap and a constant, respectively. n is a constant associated with the different types of electronic transitions ($n=1/2$, 2, $3/2$, or 3 for directly allowed, indirectly allowed, directly forbidden, and indirectly forbidden transitions, respectively). According to Lacomba-Perales et al [24], the molybdates with scheelite-type tetragonal structure present one directly allowed electronic transition. Thus, in our work, the $n=1/2$ value was adopted as the standard in above equation. For $n=1/2$, the energy gap E_g values are able to be determined by extrapolating the linear portion of the plot $(\alpha h\nu)^2$ vs $h\nu$ to zero absorbance. Accordingly, the calculated energy gaps of Co--00, Co--001, Co--003, Co--005, Co--007, Co--009, Co--011 samples are 4.16, 4.10, 3.97, 3.77, 3.79, 4.00 and 4.08 eV, respectively. Our calculated E_g value for Co--00 sample is close to the previous data [25]. Obviously, E_g value decreases and then increases with Co doping. When Mo^{6+} ion is substituted by Co^{2+} , the intermediate levels within the band gap is introduced. Compared with pure SrMoO_4 , the narrower band gap of Co-doped SrMoO_4 can decrease the recombination rate of photogenerated electron-hole pairs and enhance the photocatalytic activities, as discussed below.

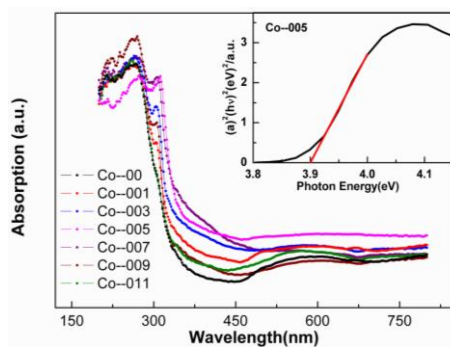


Fig. 5. UV-vis diffuse reflectance spectra for all samples, Inset plots of $(\alpha h\nu)^2$ vs photo energy ($h\nu$) for Co--005 sample.

3.5. Photocatalytic properties

The photocatalytic activities of as-prepared Co-doped SrMoO_4 samples were evaluated by the degradation of dyes MB under visible-light irradiation at room temperature. Fig. 6 shows the temporal evolution of MB solution absorption spectra under visible light irradiation for 9%Co doping SrMoO_4 sample (Co--009). It can be found that, for MB solution, the intensity of the absorption peak positioned at 654nm is decreased gradually with the increase of irradiation time.

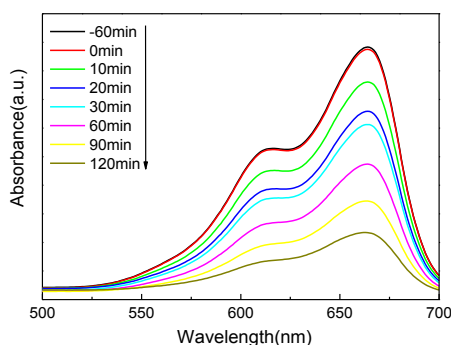


Fig. 6. Absorption spectra of MB with irradiation time over Co--009 sample.

Fig. 7 presents the variation of MB concentration (C/C_0) with irradiation time over these photocatalysts prepared with different Co doping content. The photodegradation rate of MB over pure SrMoO_4 (Co--00) was 64.8% after irradiation for 120min under the same conditions. With Co-doping in SrMoO_4 , the photodegradation rates of MB reached 64.8%, 73.1%, 81.6%, 90.8%, 85.7%, 77.2%, and 67.9% after irradiation for 120min for Co--00, Co--001, Co--003, Co--005, Co--007, Co--009, and Co--011 sample, respectively. Obviously, the photocatalytic activity of SrMoO_4 was effected by Co doping, and Co doping is helpful to enhance the photodegradation of MB resolution. In particularly, when the Co doping concentration increased from 0 to 5%, the photocatalytic activity increased, and 5% Co-doped SrMoO_4 (Co--005) showed the best degradation performance, 90.8% MB was degraded in 120min. When the doping content was over 5%, the photocatalytic activity decreases, but still better than that of pure SrMoO_4 . Our current experimental investigation clearly suggests that Co-doping is helpful to improve the photocatalytic properties of SrMoO_4 . Furthermore, there is an optical Co doping amount of the

SrMoO₄ in terms of MB photocatalytic degradation efficiency.

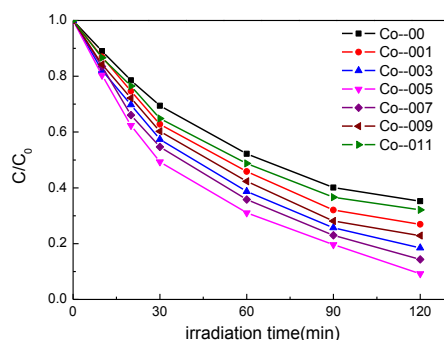


Fig. 7. The degradation rates of MB under visible light irradiation the presence for all Co-doped SrMoO₄ samples.

As we known, one proper band gap is very important to one perfect photocatalyst, because it provides energetic electron, separates photo-generated charge efficiently, and inhibits the photo-corrosion process largely [26,27]. The smaller band gap is also necessary to allow for efficient absorption overlap with the solar spectrum. This is very obligatory for the photocatalyst to effectively utilize the solar energy [28,29]. The UV-vis spectrum result also indicates, the band gaps of our obtained samples become lower with Co doping. Therefore, it is reasonable to conclude that the higher photocatalytic properties of these Co-doped samples may be related to the lower band gap.

When Co-SrMoO₄ photocatalyst is activated under irradiation, the electrons(e⁻) in the valence band (VB) are stimulated to the conduction band (CB), with the same amount of holes (h⁺) left in the VB. The electrons of the VB will be caught by O₂ adsorbed on the surface of Co-doped SrMoO₄ acting as active sites to produce ·O₂⁻ superoxide radicals. Meanwhile, the photogenerated holes of the VB can react with H₂O and OH⁻ to generate ·OH hydroxyl radicals as strong oxidizing agents. At the same time, when Co element is doped into SrMoO₄, the energy level may be formed in the middle of VB and CB. The electrons could be captured by trapping sites Co²⁺ ions, which is also helpful for separation efficiency of photo-generated charge carriers. And with increasing Co doping content, more and more electrons and holes participate in the photocatalytic process, as a result, higher photodegradation rate for MB is achieved. However, when the amount of Co doping is higher than its optimum amount of doping, excessive Co²⁺ ions may be the center of electron-hole pair recombination, thus, the photocatalytic activity is lowered for Co--007, Co-009 and Co--011 samples. A plausible electron transfer and degradation mechanism of MB over SrMoO₄ is tentatively proposed, as displayed in Fig. 8.

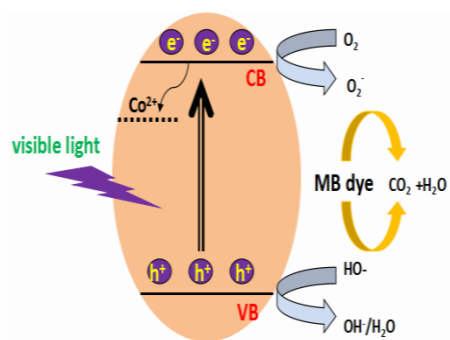


Fig. 8. Schematic diagram of charge carrier transfer process and possible photocatalytic mechanism of Co-SrMoO₄ nanoparticles.

The electrons in the CB react with the absorbed O₂ in the surface of SrMoO₄ and produce superoxide anion radicals ($\bullet\text{O}_2^-$). Simultaneously, the VB holes remaining on the VB react with H₂O/OH⁻ to generate hydroxyl radical species ($\bullet\text{OH}$). The $\bullet\text{O}_2^-$ and $\bullet\text{OH}$ could oxidize the dye molecule of MB to CO₂, H₂O, and other micromolecules. The Co doping reduces the recombination of photo-induced electrons and holes and prolong the lifetime of the electron pairs, as a result, the photocatalytic activity is enhanced due to Co doping.

4. Conclusion

In the current research, Co-doped SrMoO₄ samples are successfully synthesized by hydrothermal method. The structural, microphology, and photocatalytic properties have also systematically probed. XRD patterns reveal the crystal structure does not change. The UV-vis absorption analysis of our samples exhibits E_g value decreases from 4.16 to 3.77 eV with Co doping, which is associated with the presence of intermediary energy levels within the band gap. The photo-degradation efficiency of the as-prepared samples is also investigated by degrading of MB under visible light irradiation.

The experimental results indicate that Co doping enhances photocatalytic activity, and 5% Co-doped SrMoO₄ shows the optimal photocatalytic performance in the degradation of MB. The enhancement of photocatalytic activity is attributed to the smaller band gap and the introduction of intermediary energy levels, which decreases the recombination rate of photo-induced electrons and holes and prolongs the lifetime of carriers with Co doping. As a result, the photocatalytic activity is improved.

Acknowledgments

This work was financially supported by the National Natural Science Foundation of China under Grant no.11204001, Key Research and Development Projects of Anhui Province (1804A09020096), and the Higher Educational Natural Science Foundation of Anhui Province (KJ2017A534).

References

- [1] R. Z. Zhuang, G. F. Wang, *Optics Express* **24**, 7543(2016).
- [2] S. K. Sharma, S. Dutta, S. Som, P. S. Mandal, *Journal of Materials Science Technology* **29**, 633 (2013).
- [3] L. Krishna Bharat, Soo Hyun Lee, Jae Su Yu, *Materials Research Bulletin* **53**, 49 (2014).
- [4] B. K. Maji, H. Jena, R. Asuvathraman, K. V. G. Kutty, *Journal of Alloys and Compound* **640**, 475 (2015).
- [5] X. Y. Li, M. B. Dong, F. F. Hu, Y. G. Qin, L. Zhao, X. T. Wei, Y. H. Chen, C. K. Duan, M. Yin, *Ceramics International* **42**, 6094 (2016).
- [6] Y. N. Zhu, G. H. Zheng, Z. X. Dai, L. Y. Zhang, J. J. Mu, *Journal of Materials Science and Technology* **32**, 1361 (2016).
- [7] G. Ouyang, G. W. Yang, C. Q. Sun, W. G. Zhu, *Small* **4**, 1359 (2008).
- [8] Z. F. Yao, G. H. Zheng, Z. X. Dai, L. Y. Zhang, *Applied Organometallic Chemistry*, e4412 (2018).
- [9] Y. N. Zhu, G. H. Zheng, W. W. Fu, L. Y. Zhang, J. J. Mu, *Journal of Materials Science and Technology* **33**, 23 (2017).
- [10] B. Zhou, X. Zhao, H. J. Liu, J. H. Qu, C. P. Huang, *Separation Purification Technology* **77**, 275 (2011).
- [11] H. Kato, A. Kudo, *Journal of Physics Chemistry B* **106**, 5029 (2002).
- [12] Y. K. Yin, Y. Gao, Y. Z. Sun, B. B. Zhou, L. Ma, X. Wu, X. Zhang, *Materials Letter* **64**, 602 (2010).
- [13] E. Ciftiyurek, K. Sabolsky, E. M. Sabolsky, *Sensors and Actuators B: Chemical* **237**, 262 (2016).
- [14] Y. L. Geng, P. Zhang, N. Li, Z. H. Sun, *Journal of Alloys and Compounds* **651**, 744 (2015).
- [15] T. Thongtem, S. Kungwankunakorn, B. Kuntalue, A. Phuruangrat, S. Thongtem, *Journal of Alloys and Compounds* **506**, 475 (2010).
- [16] T. Thongtem, A. Phuruangrat, S. Thongtem, *Material Letters* **62**, 454 (2008).
- [17] Y. Sun, J. F. Ma, J. R. Fang, C. Gao, Z. S. Liu, *Inorganic Chemistry Communications* **14**, 1221 (2011).
- [18] R. Krishnan, J. Thirumalai, S. B. Thomas, M. Gowri, *Journal of Alloys and Compounds* **604**, 20 (2014).
- [19] H. C. Lei, X. B. Zhu, Y. P. Sun, W. H. Song, *Journal of Crystal Growth* **310**, 789 (2008).
- [20] G. J. Xing, Y. M. Li, Y. L. Li, Z. L. Wu, P. Sun, Y. Wang, C. Zhao, G. M. Wu, *Materials Chemistry and Physics* **127**, 465 (2011).
- [21] S. J. Lei, X. M. Peng, X. P. Li, Z. H. Liang, Y. Yang, B. C. Cheng, Y. H. Xiao, L. Zhou, *Materials Research Bulletin* **46**, 601 (2011).
- [22] Y. N. Zhu, G. H. Zheng, Z. X. Dai, L. Y. Zhang, J. J. Mu, *Journal of Materials Science and Technology* **32**, 1361 (2016).
- [23] D. L. Wood, J. Tauc, *Physics Review B* **5**, 3144 (1972).
- [24] R. Lacomba-Perales, J. Ruiz-Fuertes, D. Errandonea, D. Martinez-Garcia, A. Segura, *Europhysics Letter* **83**, 37002 (2008).
- [25] J. C. Sczancoski, L. S. Cavalcante, M. R. Joya, J. A. Varela, P. S. Pizani, E. Longo, *Chemical Engineering Journal* **140**, 632 (2008).
- [26] W. Li, Y. H. Deng, Z. X. Wu, X. F. Qian, J. P. Yang, Y. Wang, D. Gu, F. Zhang, B. Tu, D. Y. Zhao, *Journal of the American Chemical Society* **133**, 15830 (2011).

- [27] Y. H. Ng, A. Iwase, N. J. Bell, A. Kudo, R. Amal, *Catalysis Today* **164**, 353 (2011).
- [28] G. Tian, Y. Chen, X. Meng, J. Zhou, W. Zhou, K. Pan, C. Tian, Z. Ren, H. Fu, *Chem Plus Chem* **78**, 117 (2013).
- [29] X. Bai, L. Wang, Y. Zhu, *ACS Catalysis* **2**, 2769 (2012).